IEEE Access
Multidisciplinary | Rapid Review | Open Access Journal

Received October 7, 2019, accepted October 17, 2019, date of publication October 22, 2019, date of current version November 4, 2019.

Digital Object Identifier 10.1109/ACCESS.2019.2948839

Target Recognition of Synthetic Aperture Radar Images Based on Matching and Similarity Evaluation Between Binary Regions

CUIPING SHI, FENGJUAN MIAO, ZHAN JIN, AND YING XIA
College of Communication and Electronic Engineering, Qiqihar University, Qiqihar 161000, China

Corresponding author: Cuiping Shi (scp1980@126.com)

This work was supported in part by the National Natural Science Foundation of China under Grant 41701479 and Grant 61675051, in part by the China Postdoctoral Science Foundation under Grant 2017M621246, in part by the Postdoctoral Science Foundation of Heilongjiang Province of China under Grant LBH-Z17052, in part by the Project Plan of Science Foundation of Heilongjiang Province of China under Grant QC2018045, and in part by the Fundamental Research Funds in Heilongjiang Provincial Universities of China under Grant 135309342 and Grant 135309456.

ABSTRACT This work uses the binary target region for synthetic aperture radar (SAR) automatic target recognition (ATR). Due to the differences of physical sizes and target shapes, the region residuals among the same classes and those between different targets are distributed in different manners. The Euclidean distance transform is then performed on the region residuals to further enhance such differences, which is beneficial for correctly discriminating different targets. Based on the results, a similarity measure is formed according to the distribution characteristics of the region residuals. In addition, the designed similarity measure considers the possible variations of the target region caused by the nuisance conditions like noise corruption, partial occlusion, etc. Owing to its robustness and comprehensiveness, the similarity measure is applied to target recognition by comparing the test sample with different kinds of template classes. Experiments are undertaken on the Moving and Stationary Target Acquisition and Recognition (MSTAR) dataset under standard operating condition (SOC) and some representative extended operating conditions (EOCs), i.e., configuration variants, depression angle variation, noise corruption, resolution variation and partial occlusion. Moreover, the proposed method is examined under reduced training size and possible azimuth estimation errors for a comprehensive evaluation. The experimental results demonstrate the superiority of the proposed method in comparison with several baseline algorithms in SAR ATR.

INDEX TERMS Synthetic aperture radar (SAR), automatic target recognition (ATR), binary target region, Euclidean distance transform.

I. INTRODUCTION

Synthetic aperture radar (SAR) operates day and night to produce high-resolution images for earth observation. To properly analyze and interpretate SAR images for different applications, the computer-aided systems are designed to automatically process the massive data. Among all these techniques, automatic target recognition (ATR) has been widely researched for decades [1]. Like other image classification problem, SAR ATR aims to assign the representative features from the measured SAR images to a predetermined set of classes using some decision engines [2]. In general, features used for SAR ATR can be summarized into three categories. Geometrical features are common to see in SAR ATR algorithms, which depict the target's geometrical shape or physical sizes, e.g., width and length. Typical geometrical features include target region, contour, shadow, etc. Park et al. generated several discriminative features from the target's binary target region, which are demonstrated effective for SAR ATR [3]. Region descriptors such as Zernike moments [4], Krawtchouk moments [5] were used to analyze the binary target region for target recognition. Anagnostopulos employed the Elliptical Fourier Series (EFS) coefficients to approach the target outlines in SAR images, which were classified by SVM afterwards [6]. The target shadow is demonstrated effective for SAR target recognition by Papson and Narayanan [7]. The second kind is the projection features, which are obtained via projecting the original images

The associate editor coordinating the review of this manuscript and approving it for publication was Jeon Gwanggil.

to low-dimensional subspaces thus significantly reducing the redundancy. With mature mathematical tools, extraction of projection features became highly efficient [8]. Mishra applied principal component analysis (PCA) and linear discriminant analysis (LDA) to SAR ATR [9]. In [10], the non-negative matrix factorization (NMF) was employed to extract discriminative features for target recognition. With the development of manifold learning, more projection features were designed for the special applications in SAR ATR with good performance [11], [12]. The compressive sensing theory provides a simple but effective dimensionality reduction method, i.e., the random projection [13], [14]. The third category comprises of the scattering center features, describing the target's backscattering characteristics. In [15]–[18], the attributed scattering centers (ASCs) were validated notably effective for SAR target recognition because they could provide physical descriptions of the local structures on the target. In comparison, the outstanding merit of projection features boils down to the high efficiency of feature extraction. However, they lack clear physical meanings [8]. As a result, it is hard to evaluate their robustness to the extended operating conditions (EOCs) caused by the physical variations of the target such as configuration variants and partial occlusion. For the geometrical and scattering center features, they are capable of describing the physical characteristics of the target. However, the main disadvantage of these features is the complexity of feature extraction. Specially, the scattering centers are more difficult to extract than the typical geometrical features like target region, shadow, etc. because of the complex scattering center model [15]. Considering that EOCs are the main obstacle to SAR ATR, geometrical and scattering centers have more potential in these situations.

The decision engine (or in other words, the classifier) determines the target type by exploiting the discrimination in the extracted features. The great progress in the field of pattern recognition has provided many advanced classifiers for SAR ATR such as SVM [19]–[21], adaptive boosting (Adaboost) [22], discriminative graphical models [2], sparse representation-based classification (SRC) [23]–[26], modified polar mapping classifier [27], etc. Owing to the excellent classification performance of deep learning techniques, they become the most popular tools in the field of remote sensing image interpretation [28]. Various kinds and structures of deep learning models were used with very good performance [29]–[45]. In [30], Chen et al. developed the famous all-convolutional networks (A-ConvNet) based on the convolutional neural network (CNN) for SAR ATR. Other architectures of deep networks were designed based on the latest achievements in deep learning, e.g., ResNet [31], cascade coupled CNN [32], gradually distilled CNN [33], enhanced squeeze and excitation network (ESENet) [34], multi-stream CNN [35]. In addition, some works tried to enrich the available training samples. In [36], Ding et al. augmented the available training samples by image translation and noise addition. In [37], the noisy, multi-resolution, and occluded samples were generated to train the designed CNN. Transfer learning was employed to enhance deep learning models based on the simulated samples from CAD models as reported in [38]. The decision fusion of multiple classifiers was also used in SAR ATR such as the combination of SVM and CNN [39], SRC and CNN [40], etc. It is believed that the deep learning methods are actually data-driven so their performance highly depends on the amount and coverage of the available training samples. As a result, when the training and test sets have notable differences, the classification performance may degrade significantly. Therefore, it is still necessary that some traditional features or classifiers are further studied and exploited, which could be used cooperatively with the deep learning models to improve the overall recognition performance of SAR ATR.

In this study, we propose a SAR ATR method via matching of binary target regions. The target region reflects the geometrical shape and some details of the target. Therefore, it could be employed to analyses the target's local variations resulted by the configuration variants, noise corruption, partial occlusion, etc. as validated in previous works. In addition, as the region feature, the target region is more stable than the point patterns (e.g., scattering centers). For a test sample, its target region is matched with its counterparts from different template classes. The resulted region residuals reflect their differences. The region residuals of the same class (denoted as the intra-class residuals) are distributed in small and narrow patches whereas those between different targets (denoted as the between-class residuals) are in bulky shapes with large area. Hence, the distribution characteristics of the region residuals can be effectively used to distinguish different classes of targets. However, such qualitative descriptions may not be directly understood by the computer. As a remedy, the Euclidean distance transform [46]–[48] is employed to amplify and reflect such characteristics, which can be quantitatively evaluated by the computer. After the Euclidean distance transform, the intra-class residuals produce a gray image with lower intensities and the resulted gray images of the between-class residuals contain higher-value pixels. Consequently, the differences between the intra-class residuals and between-class residuals are further enhanced. By analyzing the results from Euclidean distance transform, a similarity measure is defined to evaluate the correlations between the test image and various kinds of template images. The similarity measure considers the distribution of the region residuals and the possible region deformations in a comprehensive way. Therefore, it can robustly reveal the true target label of the test sample. Compared with the projection features, the binary target region has clear physical meanings thus it is capable of sensing the local structural variations occurred to the target. Unlike other region features-based methods like [4]–[6], the proposed method directly matches the binary target regions with no further feature construction. Therefore, more discriminability contained in the target region can be maintained and exploited for target recognition. Extensive experiments are undertaken on the public Moving and Stationary Target Acquisition and Recognition (MSTAR)

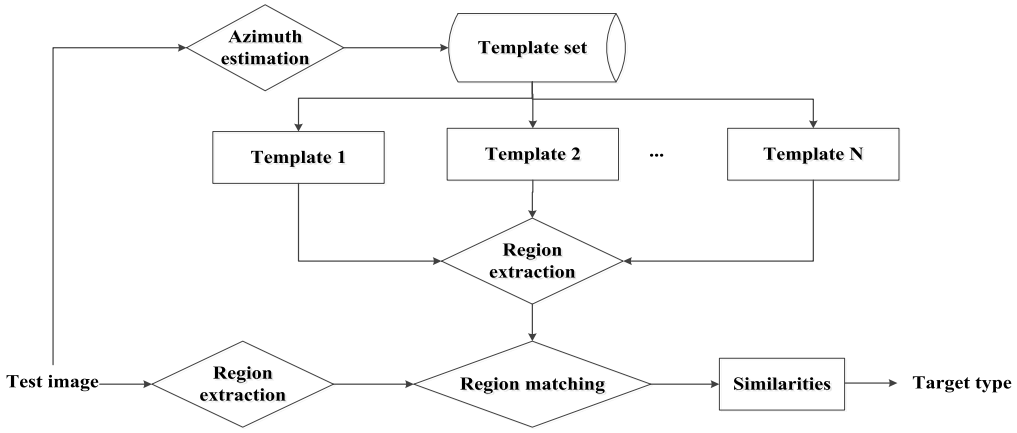

FIGURE 1. Procedure of the proposed target recognition method.

dataset under the standard operating condition (SOC) and representative EOCs including configuration variants, large depression angle variation, noise corruption, resolution variation, and partial occlusion. In addition, as a thorough evaluation, the proposed method is examined under reduced training size and possible azimuth estimation errors. According to the experimental results, the proposed method achieved superior performance over some baseline algorithms drawn from current literatures.

The remainder of this paper is organized as three sections. Section 2 introduces the methodology of the proposed method including the target region extraction, region matching, similarity definition, and detailed implementation of target recognition. Experiments are undertaken on the MSTAR dataset in Section 3 based on different experimental setups for performance evaluation. Finally, some major conclusions are summarized in Section 4 as well as some discussion

II. METHODOLOGY

Fig. 1 illustrates the main components and work flow of the proposed method. The binary target region in SAR image is first extracted using a classical target segmentation method. Afterwards, the region matching is performed based on the Euclidean distance transform. Finally, a similarity measure is deduced with application to target recognition. Therefore, the key techniques in the proposed method include the reliable region extraction, robust region matching and similarity evaluation. In the followings, these techniques are described and each step in the target recognition is also explained.

A. TARGET SEGMENTATION

Target segmentation is first performed to extract the binary target region. The target segmentation in our work is conducted based on the basic idea of the method in [22], which was also used in some relevant literatures [5], [11]. We perform the target semination in this paper according to Algorithm 1.

Algorithm 1 Target Segmentation Algorithm

Input: SAR image I

1. Normalize the image intensities in I as $\bar{I}$ via the standard histogram equalization.
2. Smooth the normalized image as $\bar{I}_*$ using a 3×3 mean filter.
3. Preliminarily segment $\bar{I}_*$ with a threshold T_1.
4. Remove the false alarms in the preliminary binary region by morphological opening operation [49], [50].
5. Connect the target region from Step 4 by morphological closing operation.

Output: The binary target region in I.

Fig. 2 gives an intuitive illustration on the target segmentation algorithm. In this case, the threshold for preliminary segmentation is set to be $T_1 = 0.8$. Fig. 2 (a) shows a BMP2 SAR image in the MSTAR dataset and the normalized image via the standard histogram equalization is shown as Fig. 2 (b). After the mean filter, the result is shown in Fig. 2 (c), in which the image intensities are smoothed. The preliminary threshold segments the smoothed image as the binary regions in Fig. 2 (d), in which some false alarms are existing due to the background clutters. The following morphological operations remove these false alarms (Fig. 2 (d)) and connect the target region to obtain the final binary target region (Fig. 2 (e)).

A further validation of the target segmentation is conducted under noise corruption and resolution variance as shown in Fig. 3 and 4, respectively. In Fig. 3, the image in Fig. 2 (a) is contaminated by the additive complex Gaussian noise (AWGN) [51], [52] with a signal-to-noise ratio (SNR) of 0dB. In this case, the target pixels still have relatively higher intensities as shown in Fig. 3 (a). Therefore, it is predictable that the target region can be segmented with a relatively high precision. Next, the morphological operations effectively reduce the false alarms brought by the noises and connect the fractured target region. Fig. 3 (b) shows the segmented target region, which shares a quite similar shape

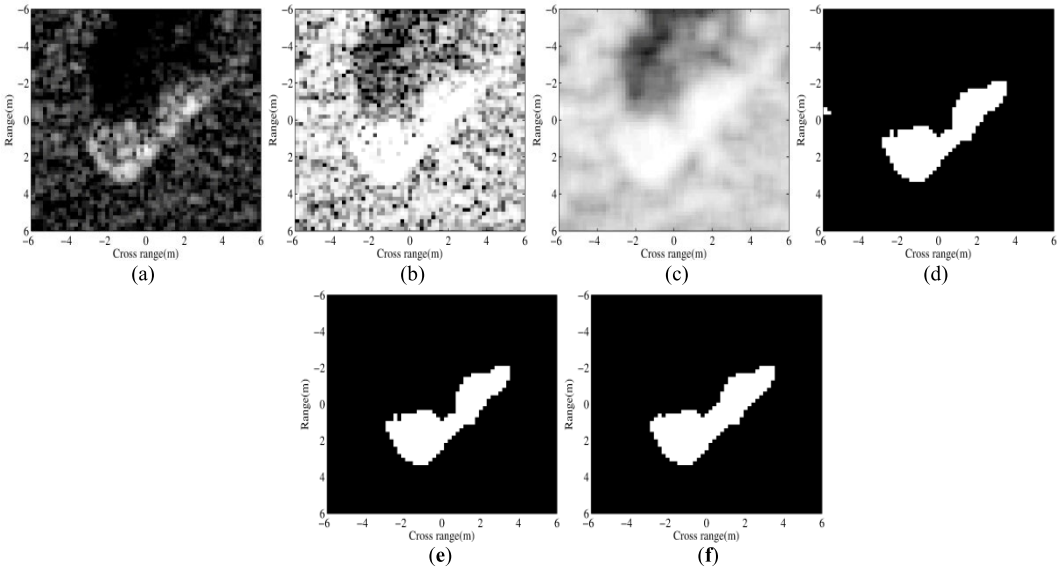

FIGURE 2. Target segmentation procedure: (a) Original image; (b) normalization via the standard histogram equalization; (c) smoothing by mean filter; (d) preliminary segmentation; (e) morphological opening operation; (f) morphological closing operation.

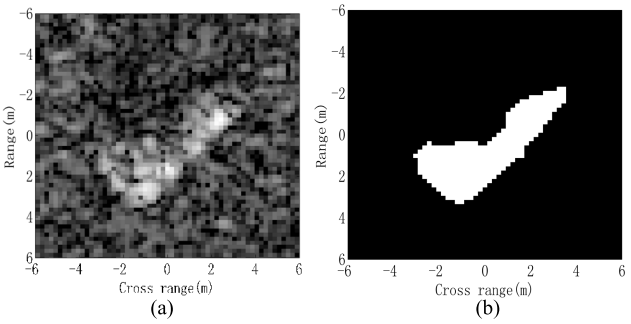

FIGURE 3. Target segmentation of noisy SAR image: (a) image at the SNR of 0dB; (b) segmented target region.

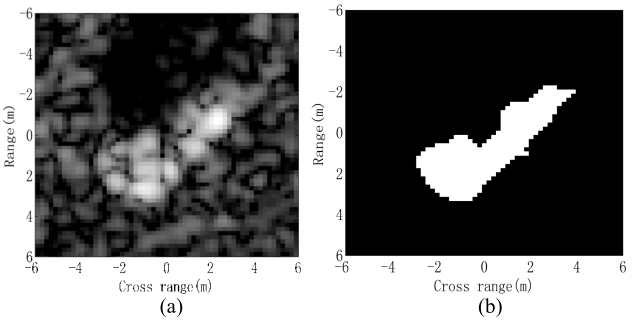

FIGURE 4. Target segmentation under resolution variance: (a) image at the resolution of 0.5m; (b) segmented target region.

with the original one in Fig. 2 (f). Fig. 4 illustrates the target segmentation under resolution variance. Fig. 4 (a) shows a SAR image with the resolution of 0.5m generated from the original image with the resolution of 0.3m. Under this situation, the dominant target region with higher intensities can be maintained as intuitively shown in Fig. 4 (a). Then, the target region can be separated out with high precision using the threshold segmentation and following morphological operations. By comparing the results in Fig. 2 (f), Fig. 3 (b) and Fig. 4 (b), it shows that the target region can keep robust under noise corruption and resolution variation. In addition, it can also sense the target's variations caused by partial occlusion. These merits will definitely contribute to the better ATR performance under different operating conditions.

B. SIMILARITY MEASURE BASED ON REGION RESIDUALS

After the target segmentation, the binary target regions of the test image and its counterpart in a certain template class as denoted as F and G, respectively. The region residuals R between the two regions are calculated as equation (1).

$$R = |F - G| \tag{1}$$

Fig. 5 shows the region residuals between a BMP2 image (shown in Fig. 2 (a)) and its corresponding template images from the MSTAR dataset. It shows that the intra-class residuals have a much smaller number of nonzero elements than that of the between-class region residuals. Denote the numbers of the nonzero pixels in F, G and R as N_F, N_G and N_R, respectively, a preliminary similarity measure is defined as equation (2) to evaluate the similarity between F and G.

$$C_0 = 1 - \frac{N_R}{N_F + N_G} \tag{2}$$

Due to the differences of the physical sizes and target shapes, the intra-class residuals are often distributed in narrow regions with small areas. In contrast, the between-class residuals are often bulky shaped with large areas as shown

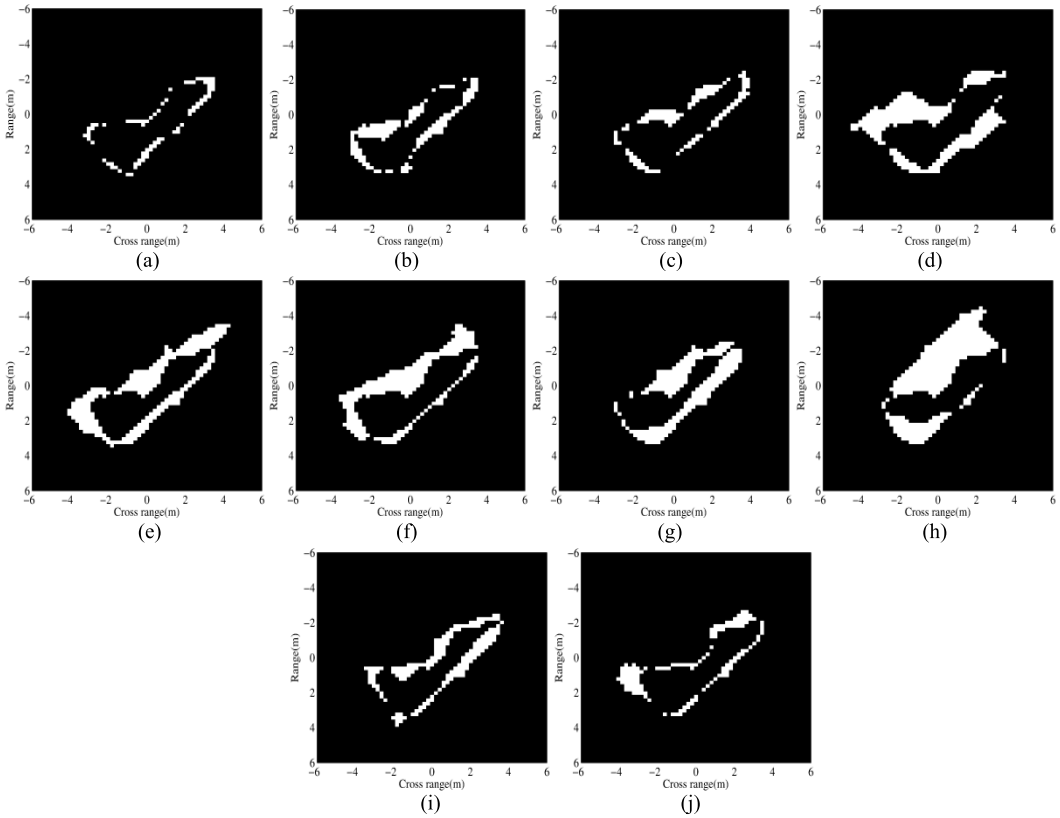

FIGURE 5. Region residuals between a BMP2 target and its corresponding templates: (a)BMP2; (b)BTR70; (c)T72; (d)ZSU23/4; (e)ZIL131; (f)T62; (g) BTR60; (h)D7; (i) BRDM2; (j) 2S1.

in Fig. 5. Then, according to the similarity measure in equation (2), a test image is assumed to share the largest similarity with its corresponding template class. However, this similarity measure only takes the area of the residuals into consideration while neglecting the distribution characteristics of the residuals. In addition, there are possible corruptions in the target region due to noise corruption, partial occlusion, etc. Therefore, a more robust similarity measure should be further designed to fully make use of binary target region to improve the classification performance.

C. RESIDUALS PROCESSING USING EUCLIDEAN DISTANCE TRANSFORM

Distance transform [46]–[48] has been widely used in image processing, such as the skeleton extraction and shape matching. For a binary image $A = [a_{xy}]$ with M rows and N columns, where a_{xy} denotes the pixel at the location of (x, y). Those pixels with $a_{xy} = 1$ are the target points, denoted as $T = \{(x, y)|a_{xy} = 1\}$. On the contrary, pixels with $a_{xy} = 0$ represent the background points, denoted as $B = \{(x, y)|a_{xy} = 0\}$. The distance transform of A is a gray image recording the minimum distance between each target point in T and all the background points. As for the Euclidean distance transform, the distance measure is chosen to be the Euclidean distance. Then, for the target point $(i, j) \in T$, its corresponding intensity in the gray image is calculate as equation (3).

$$d_{ij} = \min \{D[(i, j), (x, y)], (x, y) \in B\} \tag{3}$$

where $D[(i, j), (x, y)] = \sqrt{(i - x)^2 + (j - y)^2}$ denotes the Euclidean distance. Fig. 6 shows the corresponding Euclidean distance transforms of the region residuals in Fig. 4.

According to the distribution characteristics of the region residuals, the Euclidean distance transform of the between-class residuals have more pixels with higher values than that of the intra-class residuals as shown in Fig. 6, where all the subfigures are shown in the same dynamic range. The values of the pixels in these subfigures can be referred to the color bars at the bottom. Denote the Euclidean distance transform of the region residuals as I, the similarity measure is designed as equation (4) by modifying equation (2).

$$C_1 = 1 - \frac{Sum(I)}{N_F + N_G} \tag{4}$$

As a practical consideration, the target is probably to be occluded by the nearby obstacles such as trees or buildings. Consequently, the target region is severely deformed. Assuming the occlusion always occurs from a fixed direction, then most of the intra-class residuals are still in narrow distributions with quite a few bulky regions. Such property can be reflected by the values of the pixels on the ridge of the Euclidean distance transform. The intensities of the ridge

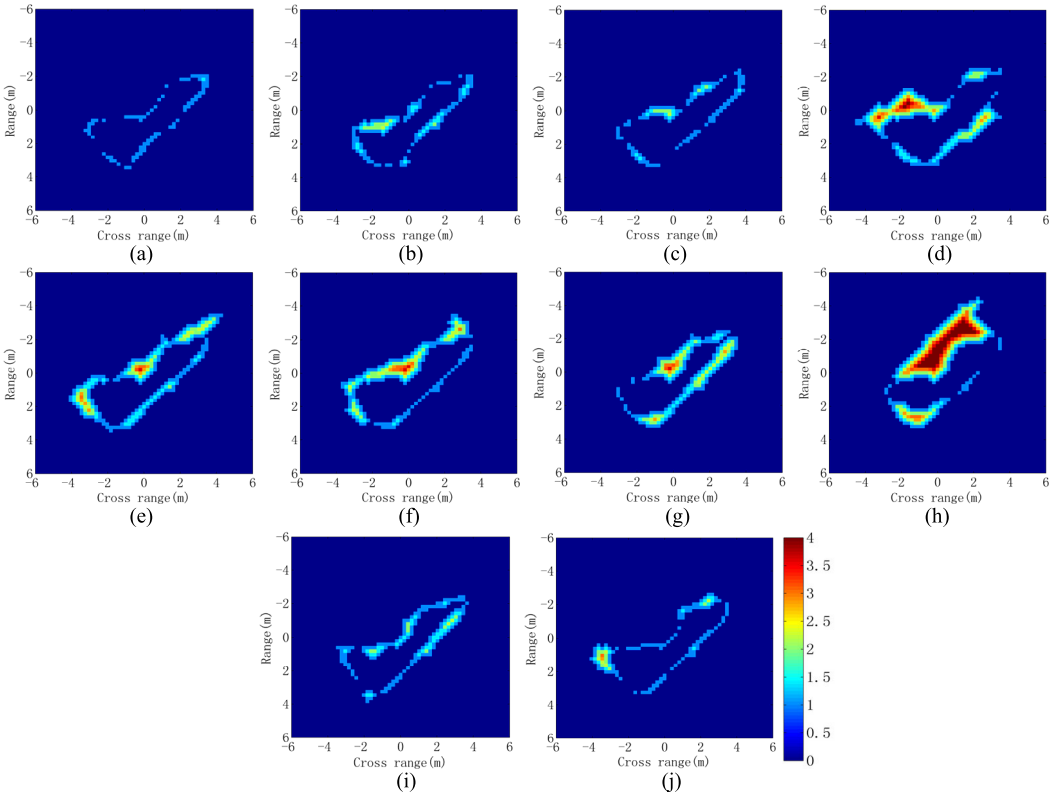

FIGURE 6. Euclidean distance transforms corresponding to the region residuals in Fig. 2: (a) BMP2; (b)BTR70; (c)T72; (d)ZSU23/4; (e)ZIL131; (f)T62; (g) BTR60; (h)D7; (i) BRDM2; (j) 2S1.

TABLE 1. Evaluation of different similarity measures.

Similarity type	Target class										J
	BMP2	BTR70	T72	ZSU23/4	ZIL131	T62	BTR60	D7	BRDM2	2S1	
C_0	0.88	0.75	0.81	0.66	0.63	0.68	0.61	0.55	0.72	0.80	0.18
C_1	0.87	0.71	0.79	0.48	0.50	0.55	0.45	0.13	0.68	0.76	0.31
C_2	0.79	0.58	0.68	0.35	0.37	0.45	0.35	0.08	0.58	0.64	0.34

pixels in the Euclidean distance transform actually reflect the width of the residual at a certain position. Therefore, the variance of the ridge pixels embodies the regularity of the residual distributions. The resulted variance of the correct target classes is lower than that from the incorrect class even there may be some region deformations. Consequently, the ridge pixels of the Euclidean distance transform of between-class residuals varies more intensively than that of the intra-class residuals. Therefore, the variance of the normalized ridge pixels σ^2 is calculated to incorporate into the final similarity measure as follow:

$$C_2 = C_1 * \exp(-\sigma^2/2) \tag{5}$$

By performing the three similarities measures on the residuals in Fig. 5, the similarities between the BMP2 image and the ten template classes from the MSTAR dataset are summarized in Table 1. Compared with similarities at C_0, those at C_1 decrease disproportionately. The similarity of the true class (BMP2) has the lowest decrease compared with the other classes. The similarities by C_2 share a similar trend with those by C_1. Consequently, the differences between the intra-class similarities and between-class similarities are enhanced, which is beneficial for the correct target recognition. To evaluate the three similarity measures quantitatively, a judgment variable is defined as equation (6), which describes the difference between the maximum similarity and the remaining ones. A larger J indicates that the similarity measure is more robust for target recognition because it can reflect the differences between the true class and confusing targets more significantly. According to the results in Table 1, C_2 is assumed to be the most effective for target recognition with the highest J. In addition, it takes the possible variations in the target region into consideration, which may be caused by severe noise corruption, partial occlusion, etc.

$$\begin{aligned} S_k &= \max([S_i]) \\ J &= S_k - \text{mean}([S_j]) \quad j \neq k \end{aligned} \tag{6}$$

FIGURE 7. Optical images of the ten targets.

TABLE 2. Template/training and test sets used for SOC recognition problem.

Class	Serial No.	Template/Training set		Test set	
		Depression	No. Images	Depression	No. Images
BMP2	9563	17°	233	15°	195
	9566	17°	232	15°	196
	c21	17°	233	15°	196
BTR70	c71	17°	233	15°	196
T72	132	17°	232	15°	196
	812	17°	231	15°	195
	S7	17°	228	15°	191
ZSU23/4	D08	17°	299	15°	274
ZIL131	E12	17°	299	15°	274
T62	A51	17°	299	15°	273
BTR60	k10yt7532	17°	256	15°	195
D7	92v13015	17°	299	15°	274
BDRM2	E71	17°	298	15°	274
2S1	B01	17°	299	15°	274

Algorithm 2 Target Recognition Algorithm

Input: SAR image I

1. Estimate the target azimuth of I using the method in [22].
2. The template set finds these template images with the most approaching azimuths with the estimated one.
3. Extract the binary target regions of the test image and the selected template images.
4. Calculate the similarities between the test target region and template target regions according to equation (6).
5. Decide the target label as the template class with the maximum similarity.

Output: The target label of I.

D. TARGET RECOGNITION

The defined similarity measure in equation (6) is used for target recognition in this work. By comparing the similarities calculated from different classes of templates, the target label of the test sample is classified as the one with the highest similarity.

The azimuth estimation method in [22] directly performs on the binary target region thus suitable to be used in this paper. In the practical application, considering the azimuth estimation errors, the template samples are selected in an azimuth range of $[-3°, 3°]$ around the estimated one. The average of the similarities of the selected samples from a certain class is used as the final similarity for target recognition.

III. EXPERIMENTS

A. PREPARATION

In order to validate the effectiveness of the proposed method, experiments are undertaken on the MSTAR dataset, which is widely taken as the benchmark for evaluating SAR ATR algorithms. The dataset includes SAR images measured from 10-class ground targets: BMP2, BTR70, T72, ZSU23/4, ZIL131, T62, BTR60, D7, BRDM2, and 2S1, which can be categorized as tank, armored car, cannon, truck, and bulldozer. The optical images of the ten targets are displayed as Fig. 7. Table 2 presents the template/training and test sets for SOC. SAR images at 17° depression angle are used as the reference samples while those at 15° are classified. The original MSTAR images have a fixed resolution of 0.3m × 0.3m with 128 × 128 pixels.

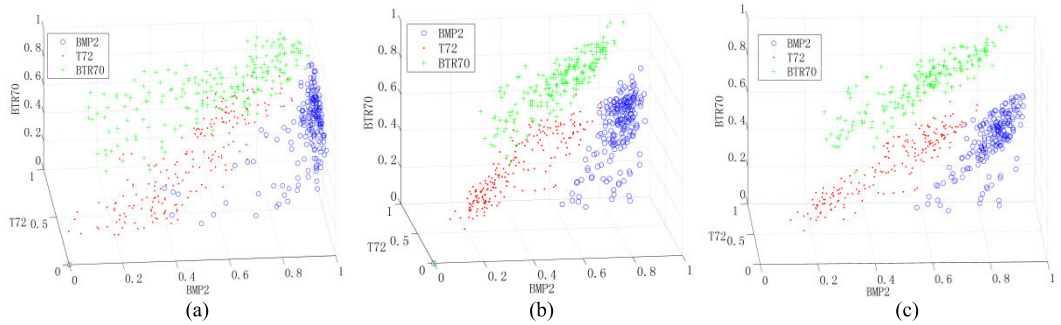

FIGURE 8. Similarity distributions of the 3-class test samples under different types of similarity. (a) C_0 (b) C_1 (c) C_2.

TABLE 3. Reference methods to be compared with the proposed one.

Abbreviation	Classifier	Feature	Reference
Zernike	SVM	Zernike moments	[4]
EFS	SVM	EFS coefficients	[6]
SVM	SVM	PCA features	[19]
SRC	SRC	PCA features	[23]
ASC	ASC Matching	ASCs	[18]
A-ConvNet	A-ConvNet	Image intensities	[30]
ResNet	ResNet	Image intensities	[31]
ESENet	ESENet	Image intensities	[34]

For comparison, several baseline SAR ATR algorithms from public literatures are used as reference methods. The descriptions of the reference methods are summarized in Table 3 including the features and decision engines. For simplicity, each of them is given an abbreviation according to the features or classifier. The Zernike [4] and EFS [6] methods were both applied on the binary target regions, which first extracted features to represent the binary target region and ten used SVM to perform target classification. The SVM [19] and SRC [23] methods were performed on the 60-dimension PCA features, which were the most prevalent classifiers used in SAR ATR so far. The ASC matching method in [18] was employed for comparison, where a similarity measure was defined to evaluate the similarity between two ASC sets for SAR ATR. Three deep learning-based methods are chosen including A-ConvNet [30], ResNet [31], and ESENet [34], which designed different architectures for target classification of SAR images. By comparison with these classical or latest works in SAR ATR, the effectiveness and robustness of the proposed method can be quantitively evaluated.

In the followings, the recognition performance of the proposed method is first evaluated under SOC. Afterwards, several typical EOCs including configuration variants, large depression angle variance, noise corruption, resolution variation, and partial occlusion are setup to test the robustness of the method. Finally, we test the proposed method under reduced training size and possible azimuth estimation errors.

B. RECOGNITION UNDER SOC

Under SOC, the operating conditions of the test samples are similar with those of the template/training samples. Therefore, it is predictable that the target recognition methods could achieve relatively good performances under SOC. The 3-class recognition and 10-class recognition problems are two classical experimental setups based on the MSTAR dataset.

1) 3-CLASS RECOGNITION PROBLEM

The 3-class recognition is first considered, where the three targets, i.e., BMP2, BTR70 and T72 are used. For each target, only one serial is used, i.e., 9563 for BMP2, c71 for BTR70, and 132 for T72. Therefore, it is a pure SOC in this condition because the test and template samples only have a small depression angle difference of 2°. Fig. 8 shows the similarity distributions of the 3-class test samples under different types of similarity measures defined in this paper, i.e., C_0, C_1 and C_2. The coordinates in Fig. 8 represent the similarity with the corresponding target class. It is clear that each of the three similarity measures can correctly discriminate the three classes with high probabilities. As we intuitively shown in Fig. 8, the similarity measures C_1 and C_2 have comparable separability for the three targets, which is consistent with the results in Table 1. In comparison, C_0 has the lowest discriminability for separating the three targets.

By comparing the similarities between the test samples and different template classes, the results of the proposed method for the 3-class recognition are summarized in Table 4. All the three targets can be recognized with the PCCs (percentage of correct classification) higher than 98% with an average of 98.81%. The PCCs of different methods for the 3-class recognition are listed in Table 5 for comparison. The A-ConvNet, ResNet, and ESENet achieve the first three highest PCCs mainly because of the good feature learning and classification abilities of deep learning models when the test samples are obtained under similar conditions with the training ones. With a PCC of 98.81%, the proposed one is more

TABLE 4. Results of the proposed method for 3-class recognition.

	BMP2	BTR70	T72	PCC (%)
BMP2	192	0	3	98.46
BTR70	0	196	0	100
T72	2	1	193	98.47
Average (%)		98.81		

TABLE 5. PCCs of different methods for 3-class recognition.

Method	Proposed	Zernike	EFS	SVM	SRC	ASC	A-ConvNet	ResNet	ESENet
PCC (%)	98.81	97.32	97.65	98.32	98.14	97.88	99.24	99.27	99.32

TABLE 6. PCCs and time consumptions of different methods for 10-class recognition.

Method	Proposed	Zernike	EFS	SVM	SRC	ASC	A-ConvNet	ResNet	ESENet
PCC (%)	98.13	94.12	94.25	95.84	95.19	94.86	97.38	97.84	98.02
Time consumption (ms)	123.2	165.8	173.4	101.7	93.2	352.6	127.4	135.2	143.5

effective than the remaining methods. Compared with the Zernike and EFS methods, it is clear that the proposed method could make better use of the discriminability of the binary target region to effectively improve the ATR performance.

2) 10-CLASS RECOGNITION PROBLEM

A more challenging problem under SOC, i.e., the 10-class recognition is undertaken in this part. A classical experimental setup is used for this experiment. In the template/training set, BMP2 and T72 only contain one serial, i.e., 9563 and 132, respectively. However, all the serials of the two targets are contained in the test set. Therefore, there are some configuration variances between the template and test sets. Fig. 9 gives the results of our methods for 10-class recognition. We can see that all the targets can be classified with PCCs over 95%. BMP2 and T72 are recognized with the lowest PCCs mainly because of the configuration variance in the test set. The average PCC is calculated to be 98.13%, indicating that the proposed method could maintain very good performance for recognizing the 10 classes of targets. A further comparison with the reference methods is given in Table 6 including the classification accuracy and time consumptions. It is notable that the deep learning methods including A-ConvNet, ResNet, and ESENet have slightly lower PCCs than the proposed method. Due to the configuration variance, the deep learning models have relatively lower capability to classify the different configurations in the test set thus impairing the overall performance. The time consumptions of different methods are calculated as the average time for classifying one MSTAR image. In comparison, the efficiency of the proposed method is lower than SVM, SRC mainly because of the time consumptions occurred during target segmentation. For the deep learning models, the major time consumptions lie in the training of the complex networks. For the Zernike and EFS methods, they needed further feature construction based on the binary target region so more time was consumed. The ASC matching method consumes notably higher time than other methods because the precise extraction of ASCs is a very difficult work.

According to the results under 3-class and 10-class problems, the proposed method could achieve very high recognition rates with good efficiency. Therefore, the proposed method is assumed to be capable of handing the multi-class recognition problem under SOC.

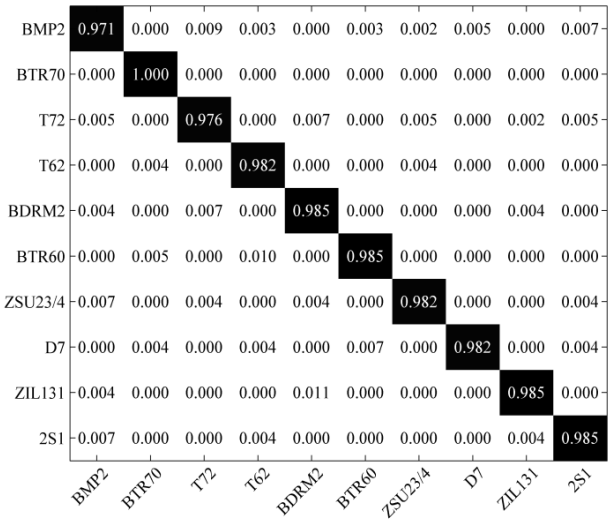

FIGURE 9. Recognition results of the proposed method for 10-class recognition.

C. RECOGNITION UNDER EOCS

In fact, many SAR ATR applications occur under EOCs due to the variations of the background environment, SAR sensors and target itself under the real-world conditions [1]. Therefore, the robustness to various EOCs is a highly desired merit of an ATR method [2]. In this subsection, the proposed method is evaluated under some representative EOCs, i.e., configuration variants, large depression angle variance, noise corruption, resolution variation, and partial occlusion.

1) CONFIGURATION VARIANTS

A certain target may be modified to have different configurations [53]. Fig. 10 shows the optical images of two

FIGURE 10. Illustration of different configurations from T72 tank: (a) A04; (b) A05.

TABLE 7. Test samples with configuration variance.

Class	Serial No.	Depression	No. Images
BMP2	9566	15°,17°	428
	c21	15°,17°	429
T72	812	15°,17°	426
	A04	15°,17°	573
	A05	15°,17°	573
	A10	15°,17°	567

configurations from T72 tank, i.e., A04 and A05, which have some modifications such as the fuel barrels. In this experimental setup, the template/training set comprises images of four targets (BMP2, BRDM2, BTR70, and T72) at 17° depression angle. For BMP2 and T72, only one serial is used, i.e., 9563 for BMP2 and 132 for T72. The test samples are summarized in Table 7, which have different configurations with the template/training ones. The results of the proposed method under configuration variance are presented in Table 8. The different configurations of BMP2 and T72 can be recognized with an average PCC of 97.46%. Table 9 compares the performances of different methods under configuration variants. We can see that the proposed method defeats the reference methods significantly. The same target with different configurations may have some local modifications, but the whole target shape can be kept. Therefore, the proposed region matching method can still work with high effectiveness. Similarly, the Zernike and EFS methods, which also perform on the target region, achieve better performance than SVM, SRC and, the deep learning-based methods. The ASC method analyzes the local characteristics of the target thus ranking second in all the methods.

2) LARGE DEPRESSION ANGLE VARIANCE

The view angle between the SAR sensor and target are always changing with the moving of the platform. Consequently, the test samples may have different depression angles with the template/training ones. As illustrated in [20], [54], SAR images measured at different depression angles tend to have notably different shapes and shadows. Then, it is a challenging but crucial issue is to enhance the robustness of the SAR ATR methods to large depression angle variance. In

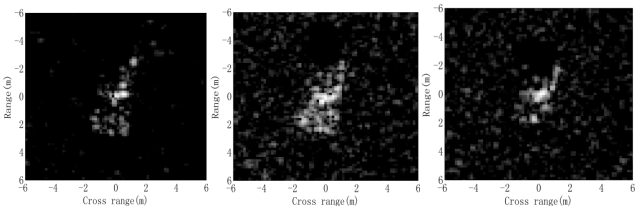

FIGURE 11. Illustration of 2S1 SAR images at different depression angles. (a) 17° (b) 30° (c) 45°.

the present test, the images of three targets (2S1, BRDM2, and ZSU23/4) at 17° depression angle are included in the template/training set. The test samples with large depression angle variance are listed in Table 10. Fig. 11 shows SAR images of 2S1 at 17°, 30°, and 45° depression angles, respectively. The PCCs of different methods are presented in Table 11, which are compared at different depression angles. When the depression angle is 30°, the test samples can still maintain relatively high resemblance with the training ones as shown in Fig. 11. Consequently, all the methods still achieve high PCCs over 95%. However, when the depression angle changes to 45°, all the performance degrades severely. As shown in Fig. 11, the target region and shadow deform significantly at 45° depression angle compared with those at 17°. As a result, the global features, e.g., PCA features, extracted from the whole image intensities contain more confusion information, which may impair the ATR performance. That is why SVM and SRC have the very low PCCs. For the deep learning models, the images for training have many differences with the test ones especially at the depression angle of 45°. As a result, its performance is much worse than the proposed method in this condition. In comparison, the highest PCCs at both depression angles are achieved by our method, indicting its superior performance when the depression angle changes greatly.

3) NOISE CORRUPTION

Considering the noises during SAR data acquisition, the SAR images to be classified may be contaminated by severe noises. To properly test the proposed method under noise corruption,

TABLE 8. Results of the proposed method under configuration variants.

Class	Serial No.	BMP2	BRDM2	BTR70	T72	PCC (%)
BMP2	9566	412	11	2	3	96.26
	c21	420	4	2	3	97.90
T72	812	18	1	0	407	95.54
	A04	5	8	0	560	97.73
	A05	1	1	0	571	99.65
	A07	3	2	3	565	98.60
	A10	7	0	2	558	98.41
Average (%)			97.46			

TABLE 9. PCCs of different methods under configuration variants.

Method	Proposed	Zernike	EFS	SVM	SRC	ASC	A-ConvNet	ResNet	ESENet
PCC (%)	97.46	95.72	95.95	93.17	92.65	96.08	95.18	95.32	95.08

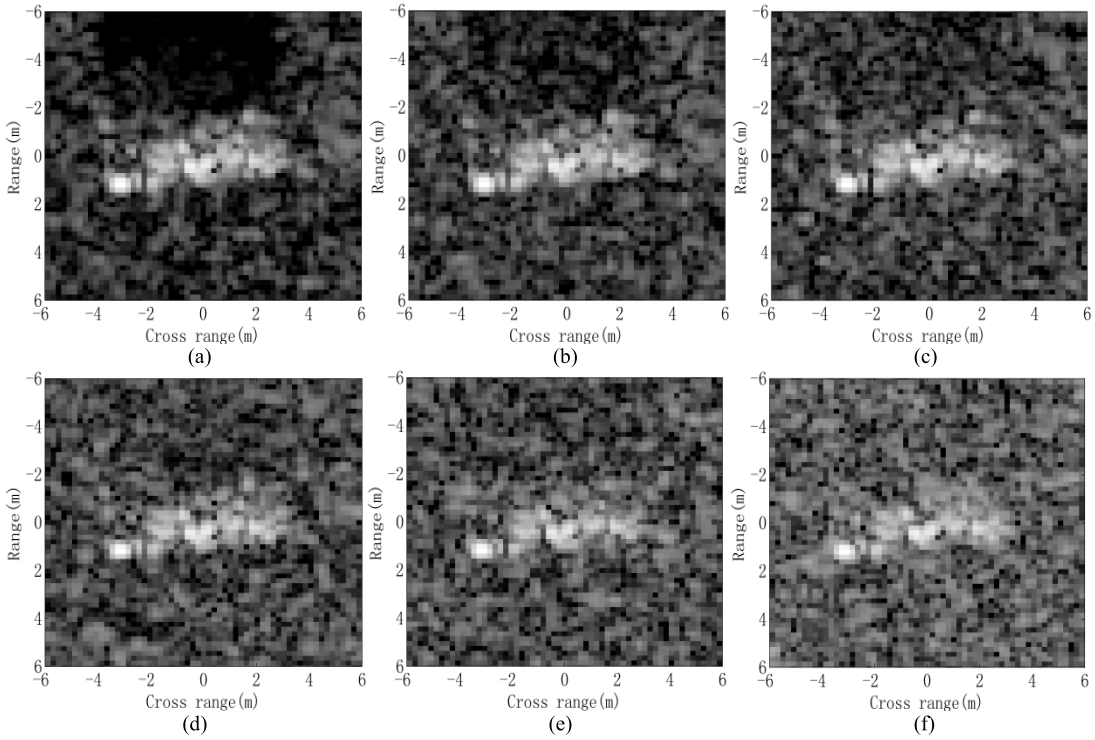

FIGURE 12. Noisy SAR images at different SNRs: (a) Original image; (b) 10dB; (c) 5dB; (d) 0dB; (e) −5dB; (f) −10dB.

TABLE 10. Test samples from different depression angles.

Class	Serial No.	Depression	No. Images
2S1	b01	30°	288
		45°	303
BRDM2	E71	30°	287
		45°	303
ZSU23/4	d08	30°	288
		45°	303

different levels of the AWGN [51], [52], [55] are added into the test samples used in the 10-class recognition problem. Some exemplar noisy SAR images are shown in Fig. 12, which are simulated at different SNRs. We can see that more target characteristics are corrupted with the deterioration of noises, causing bigger obstacles to the correct classification. Fig. 13 plots the average PCCs of different methods with the change of SNR. It clearly shows that the proposed method works most robustly under noise corruption. Although contaminated by the noises, the target pixels with high intensities can still be separated out with appropriate precision as shown in Fig. 2. Therefore, the target regions can still be matched for effective ATR. Moreover, the designed similarity measure can keep robust to possible region deformations thus better coping with the noise corruption.

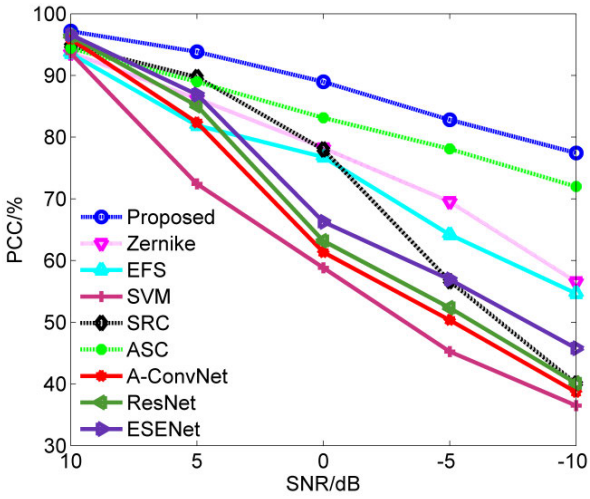

FIGURE 13. Performances of different method under noise corruption.

4) RESOLUTION VARIANCE

Due to the variation of SAR sensors, the test SAR images are possible to have some resolution variances with the template/training ones [41], [44]. To improve the applicability and generality of the SAR ATR system, the recognition

TABLE 11. Comparison of different methods under different depression angles (%).

Method		Proposed	Zernike	EFS	SVM	SRC	ASC	A-ConvNet	ResNet	ESENet
Depression	30°	97.24	95.17	95.28	96.57	96.32	96.88	96.26	96.54	96.32
	45°	73.54	65.23	62.16	56.96	59.27	58.12	68.73	69.23	68.46

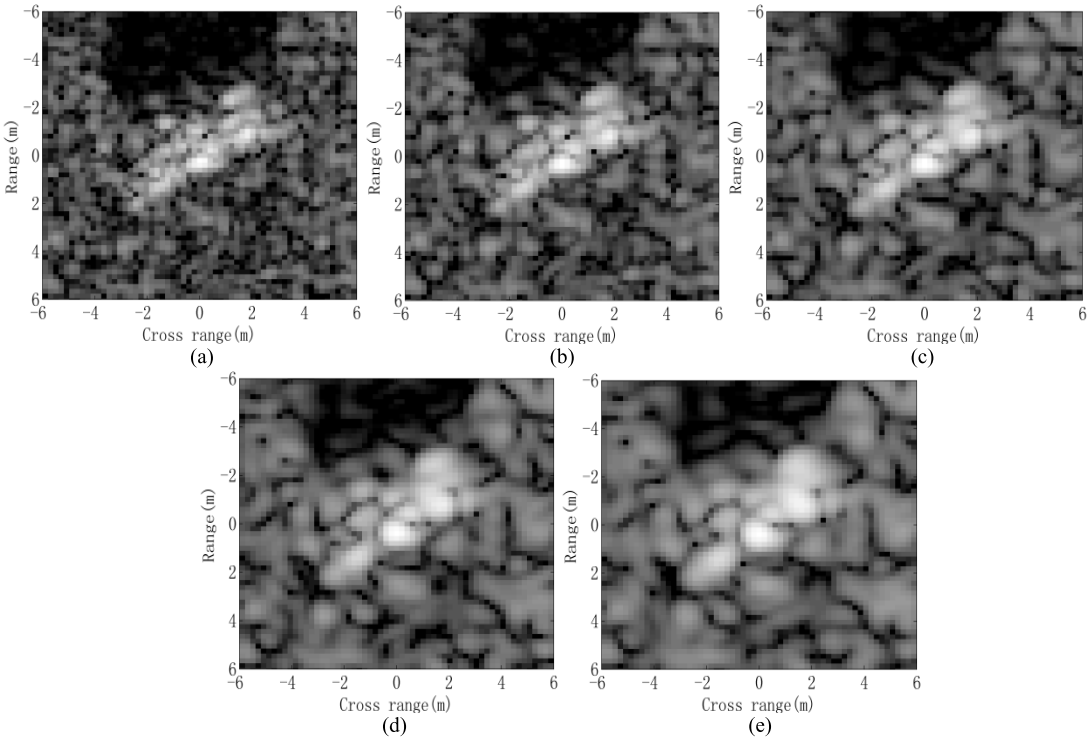

FIGURE 14. Simulated SAR images at different resolutions: (a) Original image; (b) 0.4m × 0.4m; (c) 0.5m × 0.5m; (d) 0.6m × 0.6m; (e) 0.7m × 0.7m.

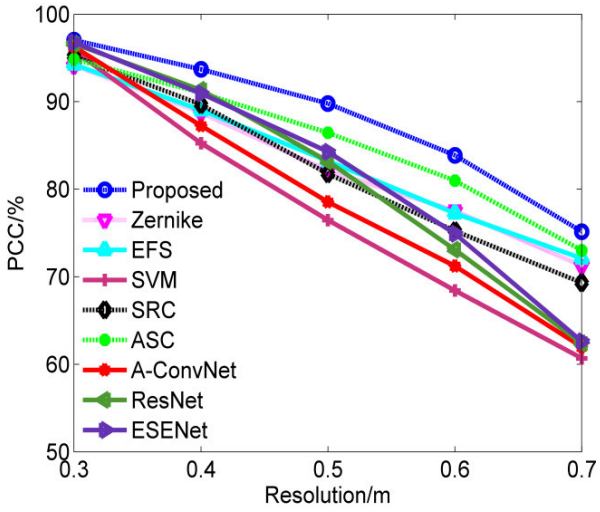

FIGURE 15. Performances of different method under resolution variation.

method should keep robust under resolution variance. In this experiment, the test samples in 10-class recognition problem are employed to simulate SAR images of different resolutions via the procedure described in [56]. Then, the multi-resolution SAR images are classified for performance evaluation. Fig. 14 shows SAR images of different resolutions. When the resolution decreases, some details on the target become more and more blurry, including the target contour and scattering centers. The PCCs of all the methods at different resolutions are plotted in Fig. 15. The proposed method achieves the highest PCC at each resolution, indicating its highest robustness to resolution variance. With large resolution differences, the PCA features change greatly. As a result, the performances of SVM and SRC decrease sharply. The deep learning models trained by the images at a fixed resolution can hardly handle the images at different resolutions. At low resolutions, the target region can still be observed with significant differences with the background pixels as validated in Fig. 3. Therefore, the proposed region matching can still be performed smoothly with good recognition performance.

5) PARTIAL OCCLUSION

Occlusion is also a common situation in SAR ATR. In this experiment, the partially occluded SAR images are first generated based on the 10-class test samples according to the occlusion model in [56], [57]. A certain percentage of the target region is removed from the original image from 8 directions. Considering the symmetry, Fig. 16 only shows 20% occluded binary target regions from 4 directions. The average PCCs of all the 8 directions for individual methods at different occlusion levels are plotted in Fig. 17. The designed similarity measure considers the possible region deformations including the partial occlusion. Therefore, it works most robustly among all the methods. In the ASC method, a one-to-one correspondence is built between the test ASC set and template ASC set thus it also has good capability of sensing the local variations like partial occlusion.

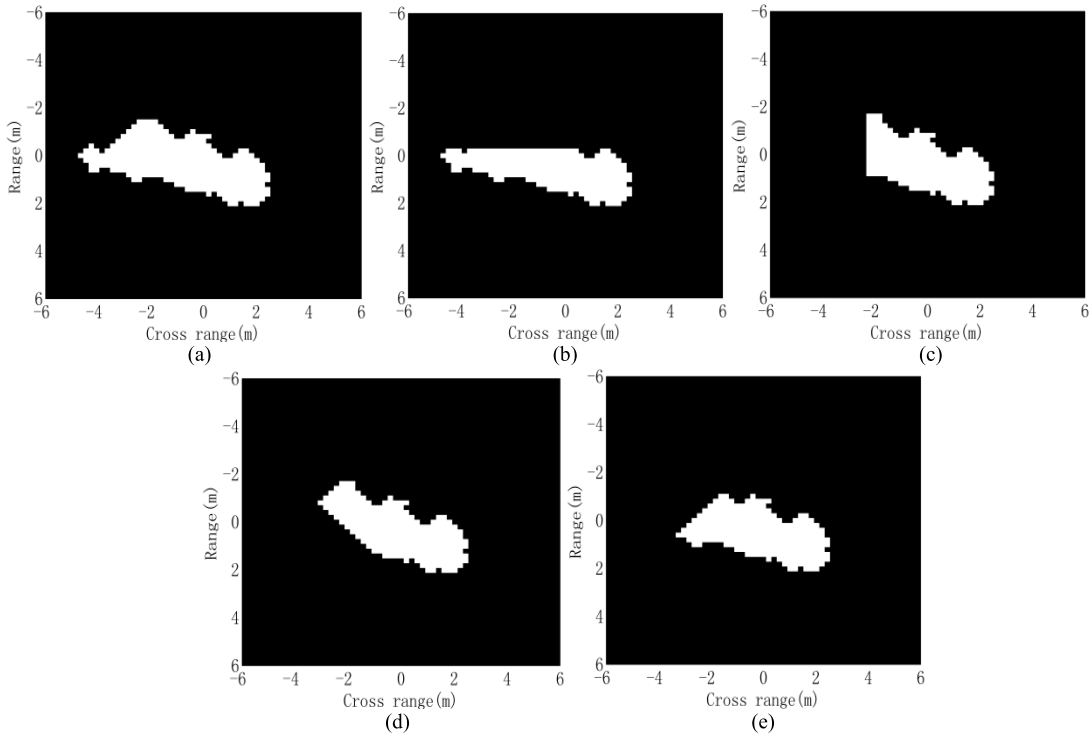

FIGURE 16. 20% occluded target region form different directions: (a) original target region; (b) direction 1; (c) direction 2; (d) direction 3; (e) direction 4.

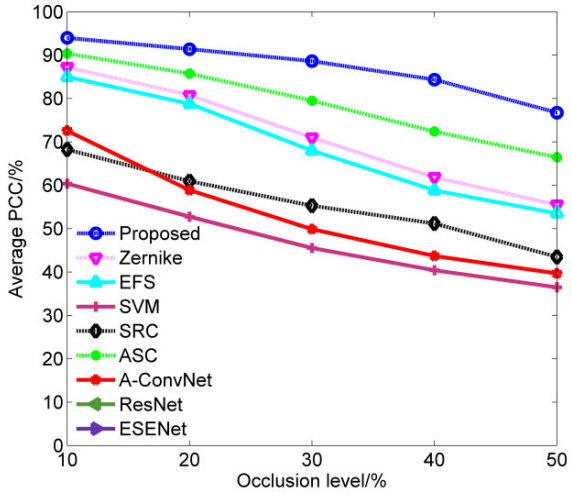

FIGURE 17. Performances of different methods under partial occlusion.

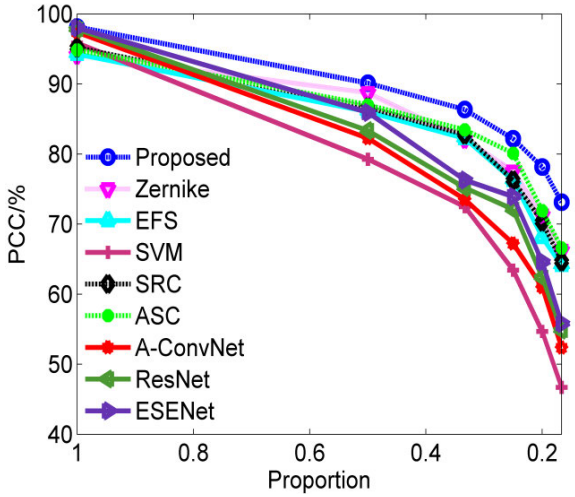

FIGURE 18. Performances of different methods under reduced training size.

D. RECOGNITION UNDER REDUCED TRAINING SIZE

Unlike optical image recognition, where a large amount of resources are available, the training samples in SAR image interpretation is notably limited [24]. Therefore, it is desired that the target recognition methods should maintain robust under reduced training size. As a simulation, this paper randomly selects 1/2, 1/3, 1/4, 1/5 and 1/6 of the template/training samples from each of the ten targets. Then, all the methods are tested under reduced training size. In order to overcome the randomness, the random selection is repeated for 10 times to obtain an average PCC. Fig. 18 compares the performance of different methods under reduced training sizes. With the highest PCC at each training size, the proposed method is validated to be the most robust. It is also clear that the performance of SVM and deep learning models degrades sharply with the decrease of the training samples. The classification capabilities of deep learning models are closely related to the coverage of training samples. SRC performs

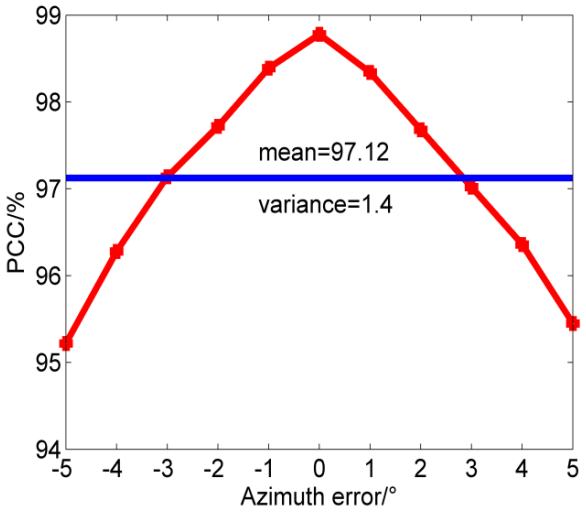

FIGURE 19. PCCs of the proposed method under azimuth estimation errors.

relatively well under reduced training size mainly because of the merit of the sparse representation as reported in [58].

E. RECOGNITION UNDER AZIMUTH ESTIMATION ERRORS

There are possibly some azimuth estimation errors during the implementation of the proposed target recognition method. SAR images are sensitive to the azimuth. Accordingly, the target azimuth can be estimated based on the binary target region, which can be effectively used to select the corresponding template samples. However, it is still a difficult problem to obtain high-precision estimations. To test the stability of the proposed method to azimuth estimation errors, some disturbances are added to the estimated azimuth. Fig. 19 shows the PCCs of the proposed method for the 10-class recognition in the azimuth error interval of $[-5°, 5°]$, which is widely adopted as the state-of-the-art precision of the azimuth estimation on MSTAR images. It shows that the proposed method maintains relatively high PCCs in the azimuth error interval. When the azimuth error is within 3°, the PCC keeps higher than the average PCC of the whole interval (marked by the blue line in Fig. 19). The reasons are mainly from two aspects. On the one hand, in the proposed method, the average similarity in an azimuth interval of $[-3°, 3°]$ is adopted as the final one thus weakening the negative influences of the azimuth estimation error. On the other hand, it is assumed the region features have better robustness to the azimuth change than the global features, scattering centers, etc. Therefore, the binary target region used in the proposed method also contributes to the superior performance of our method.

IV. CONCLUSION

This paper proposes a SAR ATR method based on the matching of target regions via Euclidean distance transform. According to the distribution characteristics of the intra-class region residuals and between-class region residuals, the Euclidean distance transform is employed to enhance the differences between the intra-class targets and between-class targets. A robust similarity is designed afterwards for target recognition, which comprehensively considers the distribution of the region residuals and the possible region deformations caused by noise corruption, partial occlusion, etc. Based on the similarity measure, the test sample is determined to be the class with the highest similarity.

To properly evaluate the proposed method, extensive experiments are undertaken on the MSTAR dataset. Experimental results reveal several conclusions as follows. First, the proposed method achieves very good performance under SOC due to the higher discriminability of the designed similarity measure. Second, the proposed method significantly outperforms other state-of-the-art SAR ATR methods under various EOCs because of the clear physical meanings of target region as well as the consideration of possible region deformations. Third, the proposed method maintains very good performance under reduced training size and possible azimuth estimation errors. Therefore, the proposed method has much potential to be used in the practical applications. Actually, the practical SAR ATR system may be a combination of different features and classifiers, which work cooperatively to improve the ATR performance. Then, the proposed method can be used in a SAR ATR system to jointly work with other ATR methods such as the CNN.

REFERENCES

[1] K. El-Darymli, E. W. Gill, P. Mcguire, D. Power, and C. Moloney, "Automatic target recognition in synthetic aperture radar imagery: A state-of-the-art review," *IEEE Access*, vol. 4, pp. 6014–6058, 2016.

[2] U. Srinivas, V. Monga, and R. G. Raj, "SAR automatic target recognition using discriminative graphical models," *IEEE Trans. Aerosp. Electron. Syst.*, vol. 50, no. 1, pp. 591–606, Jan. 2014.

[3] J.-I. Park, S.-H. Park, and K.-T. Kim, "New discrimination features for SAR automatic target recognition," *IEEE Geosci. Remote Sens. Lett.*, vol. 10, no. 3, pp. 476–480, May 2013.

[4] M. Amoon and G.-A. Rezai-Rad, "Automatic target recognition of synthetic aperture radar (SAR) images based on optimal selection of Zernike moments features," *IET Comput. Vis.*, vol. 8, no. 2, pp. 77–85, Apr. 2014.

[5] C. Clemente, L. Pallotta, D. Gaglione, A. De Maio, and J. J. Soraghan, "Automatic target recognition of military vehicles with Krawtchouk moments," *IEEE Trans. Aerosp. Electron. Syst.*, vol. 53, no. 1, pp. 493–500, Feb. 2017.

[6] G. C. Anagnostopoulos, "SVM-based target recognition from synthetic aperture radar images using target region outline descriptors," *Nonlinear Anal., Theory, Methods Appl.*, vol. 71, no. 2, pp. e2934–e2939, 2009.

[7] S. Papson and R. M. Narayanan, "Classification via the shadow region in SAR imagery," *IEEE Trans. Aerosp. Electron. Syst.*, vol. 48, no. 2, pp. 969–980, Apr. 2012.

[8] Z. He, J. Lu, and G. Kuang, "A fast SAR target recognition approach using PCA features," in *Proc. 4th Int. Conf. Image Graph.*, Aug. 2007, pp. 580–585.

[9] A. K. Mishra, "Validation of PCA and LDA for SAR ATR," in *Proc. IEEE Region Conf.*, Nov. 2008, pp. 1–6.

[10] Z. Cui, Z. Cao, J. Yang, J. Feng, and H. Ren, "Target recognition in synthetic aperture radar images via non-negative matrix factorisation," *IET Radar Sonar Navigat.*, vol. 9, no. 9, pp. 1376–1385, 2015.

[11] Y. Huang, J. Peia, J. Yanga, B. Wang, and X. Liu, "Neighborhood geometric center scaling embedding for SAR ATR," *IEEE Trans. Aerosp. Electron. Syst.*, vol. 50, no. 1, pp. 180–192, Jan. 2014.

[12] M. T. Yu, G. G. Dong, H. Y. Fan, and G. Y. Kuang, "SAR target recognition via local sparse representation of multi-manifold regularized low-rank approximation," *Remote Sens.*, vol. 10, no. 2, p. 211, 2018.

[13] A. Majumdar and R. K. Ward, "Robust classifiers for data reduced via random projections," *IEEE Trans. Syst., Man, Cybern. B. Cybern.*, vol. 40, no. 5, pp. 1359–1371, Oct. 2010.
[14] J. J. Thiagarajan, K. N. Ramamurthy, P. Knee, A. Spanias, and V. Berisha, "Sparse representations for automatic target classification in SAR images," in *Proc. 4th Int. Symp. Commun., Control Signal Process.*, Mar. 2010, pp. 1–4.
[15] L. C. Potter and R. L. Moses, "Attributed scattering centers for SAR ATR," *IEEE Trans. Image Process.*, vol. 6, no. 1, pp. 79–91, Jan. 1997.
[16] B. Ding, G. Wen, J. Zhong, C. Ma, and X. Yang, "Robust method for the matching of attributed scattering centers with application to synthetic aperture radar automatic target recognition," *J. Appl. Remote Sens.*, vol. 10, no. 1, 2016, Art. no. 016010.
[17] B. Ding, G. Wen, X. Huang, C. Ma, and X. Yang, "Target recognition in synthetic aperture radar images via matching of attributed scattering centers," *IEEE J. Sel. Topics Appl. Earth Observ. Remote Sens.*, vol. 10, no. 7, pp. 3334–3347, Jul. 2017.
[18] X. Zhang, "Noise-robust target recognition of SAR images based on attribute scattering center matching," *Remote Sens. Lett.*, vol. 10, no. 2, pp. 186–194, 2018.
[19] Q. Zhao and J. C. Principe, "Support vector machines for SAR automatic target recognition," *IEEE Trans. Aerosp. Electron. Syst.*, vol. 37, no. 2, pp. 643–654, Apr. 2001.
[20] S. A. Wagner, "SAR ATR by a combination of convolutional neural network and support vector machines," *IEEE Trans. Aerosp. Electron. Syst.*, vol. 52, no. 6, pp. 2861–2872, Dec. 2016.
[21] H. Liu and S. Li, "Decision fusion of sparse representation and support vector machine for SAR image target recognition," *Neurocomputing*, vol. 113, pp. 97–104, Aug. 2013.
[22] Y. Sun, Z. Liu, S. Todorovic, and J. Li, "Adaptive boosting for SAR automatic target recognition," *IEEE Trans. Aerosp. Electron. Syst.*, vol. 43, no. 1, pp. 112–125, Jan. 2007.
[23] H. Song, K. Ji, Y. Zhang, X. Xing, and H. Zou, "Sparse representation-based SAR image target classification on the 10-class MSTAR data set," *Appl. Sci.*, vol. 6, no. 1, p. 26, 2016.
[24] G. Dong, G. Kuang, N. Wang, L. Zhao, and J. Lu, "SAR target recognition via joint sparse representation of monogenic signal," *IEEE J. Sel. Topics Appl. Earth Observat. Remote Sens.*, vol. 8, no. 7, pp. 3316–3328, Jul. 2015.
[25] S. Song, B. Xu, and J. Yang, "SAR target recognition via supervised discriminative dictionary learning and sparse representation of the SAR-HOG feature," *Remote Sens.*, vol. 8, no. 8, p. 683, 2016.
[26] A. Karine, A. Toumi, A. Khenchaf, and M. El Hassouni, "Target recognition in radar images using weighted statistical dictionary-based sparse representation," *IEEE Geosci. Remote Sens. Lett.*, vol. 14, no. 12, pp. 2403–2407, Dec. 2017.
[27] J.-I. Park and K.-T. Kim, "Modified polar mapping classifier for SAR automatic target recognition," *IEEE Trans. Aerosp. Electron. Syst.*, vol. 50, no. 2, pp. 1092–1107, Apr. 2014.
[28] X. X. Zhu, D. Tuia, L. Mou, G.-S. Xia, L. Zhang, F. Xu, and F. Fraundorfer, "Deep learning in remote sensing: A comprehensive review and list of resources," *IEEE Geosci. Remote Sens. Mag.*, vol. 5, no. 4, pp. 8–36, Dec. 2017.
[29] D. A. E. Morgan, "Deep convolutional neural networks for ATR from SAR imagery," *Proc. SPIE*, vol. 9475, May 2015, Art. no. 94750F.
[30] S. Chen, H. Wang, F. Xu, and Y.-Q. Jin, "Target classification using the deep convolutional networks for SAR images," *IEEE Trans. Geosci. Remote Sens.*, vol. 54, no. 8, pp. 4806–4817, Aug. 2016.
[31] H. Furukawa, "Deep learning for target classification from SAR imagery data augmentation and translation invariance," Inst. Electron., Inf. Commun. Eng., Tokyo, Japan, IEICE Tech. Rep. SANE2017-30, 2017, pp. 13–17.
[32] J. Zhao, Z. Zhang, W. Yu, and T.-K. Truong, "A cascade coupled convolutional neural network guided visual attention method for ship detection from SAR images," *IEEE Access*, vol. 6, pp. 50693–50708, 2018.
[33] R. Min, H. Lan, Z. Cao, and Z. Cui, "A gradually distilled CNN for SAR target recognition," *IEEE Access*, vol. 7, pp. 42190–42200, 2019.
[34] L. Wang, X. Bai, and F. Zhou, "SAR ATR of ground vehicles based on ESENet," *Remote Sens.*, vol. 11, no. 11, p. 1316, 2019.
[35] P. Zhao, K. Liu, H. Zou, and X. Zhen, "Multi-stream convolutional neural network for SAR automatic target recognition," *Remote Sens.*, vol. 10, no. 9, p. 1473, Sep. 2018.
[36] J. Ding, B. Chen, H. Liu, and M. Huang, "Convolutional neural network with data augmentation for SAR target recognition," *IEEE Geosci. Remote Sens. Lett.*, vol. 13, no. 3, pp. 364–368, Mar. 2016.
[37] Y. Yan, "Convolutional neural networks based on augmented training samples for synthetic aperture radar target recognition," *J. Electron. Imag.*, vol. 27, no. 2, 2018, Art. no. 023024.
[38] D. Malmgren-Hansen, A. Kusk, J. Dall, A. A. Nielsen, R. Engholm, and H. Skriver, "Improving SAR automatic target recognition models with transfer learning from simulated data," *IEEE Geosci. Remote Sens. Lett.*, vol. 14, no. 9, pp. 1484–1488, Sep. 2017.
[39] Z. Cui, C. Tang, Z. Cao, and S. Dang, "SAR unlabeled target recognition based on updating CNN with assistant decision," *IEEE Geosci. Remote Sens. Lett.*, vol. 15, no. 10, pp. 1585–1589, Oct. 2018.
[40] O. Kechagias-Stamatis and N. Aouf, "Fusing deep learning and sparse coding for SAR ATR," *IEEE Trans. Aerosp. Electron. Syst.*, vol. 55, no. 2, pp. 785–797, Apr. 2019.
[41] C. Jiang and Y. Zhou, "Hierarchical fusion of convolutional neural networks and attributed scattering centers with application to robust SAR ATR," *Remote Sens.*, vol. 10, no. 6, p. 819, 2018.
[42] J. H. Cho and C. G. Park, "Multiple feature aggregation using convolutional neural networks for SAR image-based automatic target recognition," *IEEE Geosci. Remote Sens. Lett.*, vol. 15, no. 12, pp. 1882–1886, Dec. 2018.
[43] M. Kang, K. Ji, X. Leng, X. Xing, and H. Zhou, "Synthetic aperture radar target recognition with feature fusion based on a stacked autoencoder," *Sensors*, vol. 17, no. 1, p. 192, 2017.
[44] S. Tian, C. Wang, H. Zhang, and B. Bhanu, "SAR object classification using the DAE with a modified triplet restriction," *IET Radar, Sonar Navigat.*, vol. 13, no. 7, pp. 1081–1091, Jul. 2019.
[45] Y. Kwak, W. Song, and S. Kim, "Speckle -noise-invariant convolutional neural network for SAR target recognition," *IEEE Geosci. Remote Sens. Lett.*, vol. 16, no. 4, pp. 549–553, 2019.
[46] D. W. Paglieroni, "Distance transforms: Properties and machine vision applications," *CVGIP, Graph. Models Image Process.*, vol. 54, pp. 56–74, Jan. 1992.
[47] C. R. Maurer, R. Qi, and V. Raghavan, "A linear time algorithm for computing exact Euclidean distance transforms of binary images in arbitrary dimensions," *IEEE Trans. Pattern Anal. Mach. Intell.*, vol. 25, no. 2, pp. 265–270, Feb. 2003.
[48] T. E. Schouten and E. L. van den Broek, "Fast exact Euclidean distance (FEED): A new class of adaptable distance transform," *IEEE Trans. Pattern Anal. Mach. Intell.*, vol. 36, no. 11, pp. 2159–2172, Nov. 2014.
[49] R. Gonzalez and R. Woods, *Digital Image Processing*. Princeton, NJ, USA: Prentice-Hall, 2008.
[50] B. Ding, G. Wen, C. Ma, and X. Yang, "Target recognition in synthetic aperture radar images using binary morphological operations," *J. Appl. Remote Sens.*, vol. 10, no. 4, 2016, Art. no. 046006.
[51] S. Doo, G. Smith, and C. Baker, "Target classification performance as a function of measurement uncertainty," in *Proc. 5th Asia–Pacific Conf. Synth. Aperture Radar*, Sep. 2015, pp. 587–590.
[52] B. Ding and G. Wen, "Exploiting multi-view SAR images for robust target recognition," *Remote Sens.*, vol. 9, no. 11, p. 1150, 2017.
[53] M. Liu and S. Chen, "Label-dependent sparse representation for synthetic aperture radar target configuration recognition," *Int. J. Remote Sens.*, vol. 38, no. 17, pp. 4868–4887, 2017.
[54] B. Ravichandran, A. Gandhe, R. Smith, and R. Mehra, "Robust automatic target recognition using learning classifier systems," *Inf. Fusion*, vol. 8, pp. 252–265, Jul. 2007.
[55] Z. Jianxiong, S. Zhiguang, C. Xiao, and F. Qiang, "Automatic target recognition of SAR images based on global scattering center model," *IEEE Trans. Geosci. Remote Sens.*, vol. 49, no. 10, pp. 3713–3729, Oct. 2011.
[56] B. Ding and G. Wen, "Target recognition of SAR images based on multi-resolution representation," *Remote Sens. Lett.*, vol. 8, no. 11, pp. 1006–1014, 2017.
[57] G. Jones and B. Bhanu, "Recognition of articulated and occluded objects," *IEEE Trans. Pattern Anal. Mach. Intell.*, vol. 21, no. 7, pp. 603–613, Jul. 1999.
[58] J. Wright, A. Y. Yang, A. Ganesh, S. S. Sastry, and Y. Ma, "Robust face recognition via sparse representation," *IEEE Trans. Pattern Anal. Mach. Intell.*, vol. 31, no. 2, pp. 210–227, Feb. 2009.

CUIPING SHI received the Ph.D. degree from the Harbin Institute of Technology (HIT), in 2016. She is currently an Associate Professor with the Department of Communication Engineering, Qiqihar University. Her current research interests include remote sensing image processing and target recognition.

FENGJUAN MIAO received the Ph.D. degree from East China Normal University, in 2010. She is currently a Professor with the Department of Internet of Things (IOT), Qiqihar University. Her current research interests include digital image processing and image communication.

ZHAN JIN received the M.S. degree from Harbin Engineering University, in 2010. She is currently an Associate Professor with the Department of Communication Engineering, Qiqihar University. Her current research interests include adaptive signal processing and sparse representation.

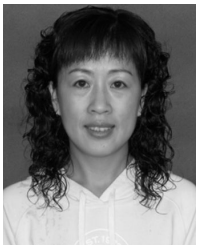

YING XIA received the Ph.D. degree from the Harbin Institute of Technology (HIT), in 2016. She is currently an Associate Professor with the Department of Communication Engineering, Qiqihar University. Her current research interests include digital image processing and pattern recognition.